THE ASTROPHYSICAL JOURNAL, 621:L1–L4, 2005 March 1
© 2005. The American Astronomical Society. All rights reserved. Printed in U.S.A.

CO (1–0) AND CO (5–4) OBSERVATIONS OF THE MOST DISTANT KNOWN RADIO GALAXY AT $z = 5.2$

I. J. KLAMER,[1,2] R. D. EKERS,[2] E. M. SADLER,[1] A. WEISS,[3] R. W. HUNSTEAD,[1] AND C. DE BREUCK[4]

Received 2004 December 16; accepted 2005 January 20; published 2005 February 9

ABSTRACT

Using the Australia Telescope Compact Array, we have detected CO (1–0) and CO (5–4) from TN J0924−2201 at $z = 5.2$, the most distant radio galaxy known to date. This is the second highest redshift detection of CO published so far. The CO (1–0) line emission is 250–400 km s^{-1} wide with a peak flux density of 520 ± 115 μJy beam^{-1}, while the CO (5–4) line emission is 200–300 km s^{-1} wide with a peak flux density of 7.8 ± 2.7 mJy beam^{-1}. Both transitions are spatially unresolved, but there is marginal evidence for spatial offsets between the CO and the host galaxy; the CO (1–0) is located 28 ± 11 kpc (4.″5 ± 1.″7) north of the radio galaxy, while the CO (5–4) is located 18 ± 8 kpc (2.″8 ± 1.″2) south of the radio galaxy. Higher spatial resolution observations are required to determine the reality of these offsets. Our result is the second detection of CO in a high-redshift galaxy without preselection based on a massive dust content.

Subject headings: early universe — galaxies: formation — galaxies: high-redshift — galaxies: individual (TN J0924−2201) — radio lines: galaxies

1. INTRODUCTION

Right out to the highest redshifts so far identified, radio galaxies are the most massive systems at each epoch. They reside in regions of overdensity (Lè Fevre et al. 1996; Carilli et al. 1997; Pascarelle et al. 1998; Pentericci et al. 2000), corroborating evolutionary models that trace high-redshift radio galaxies (HzRGs; $z > 2$) through to nearby central dominant elliptical galaxies in cluster-type environments (e.g., Lilly & Longair 1984). Unlike their nearby counterparts, however, HzRGs are not massive elliptical galaxies with old stellar populations. Instead, their rest-frame optical/UV morphologies are composed of multiple blobs of clumpy emission often aligned along the axis of relativistic jets (van Breugel et al. 1998; Pentericci et al. 1999). Rest-frame far-infrared observations are strongly suggestive of large-scale, massive, dust-obscured star formation (Stevens et al. 2003). Furthermore, HzRGS are often enshrouded by massive gas reservoirs that extend over tens of kiloparsecs, traced both by Lyα halos (McCarthy et al. 1990; Villar-Martín et al. 2003) and by carbon monoxide (CO) line emission (Papadopoulos et al. 2000; De Breuck et al. 2003). Each of these properties is consistent with the scenario where the galaxies are being observed in their formative stages. It is essential, therefore, that the characteristics of the HzRG population are investigated in detail in order to further our understanding of galaxy, and cluster, formation and evolution. In this Letter, we report the detection of molecular gas at $z = 5.2$ in TN J0924−2201, the highest redshift radio galaxy and the second highest redshift CO detection to date, after the $z = 6.42$ quasar SDSS J1148+5251 (Fan et al. 2003; Walter et al. 2003). Where necessary, we use a flat Λ-dominated cosmology with $H_0 = 71$ km s^{-1} Mpc^{-1} and $\Omega_\Lambda = 0.73$ (Spergel et al. 2003). In this cosmology, $1'' = 6.3$ kpc at $z = 5.2$.

[1] School of Physics, University of Sydney, A28, Sydney, NSW 2006, Australia; i.klamer@physics.usyd.edu.au, e.sadler@physics.usyd.edu.au, r.hunstead@physics.usyd.edu.au.

[2] CSIRO, Australia Telescope National Facility, P.O. Box 76, Epping, NSW 1710, Australia; rekers@csiro.au.

[3] Instituto de Radioastronomia Milimetrica, Avenida Divina Pastora 7, 18012 Granada, Spain; aweiss@iram.es.

[4] European Southern Observatory, Karl-Schwarzschild-Strasse 2, 85748 Garching bei München, Germany; cdebreuc@eso.org.

2. TN J0924−2201: SELECTION AND CHARACTERISTICS

TN J0924−2201 was initially discovered (De Breuck et al. 2000) from radio surveys using the well-established technique for finding HzRGs of selecting ultrasteep spectrum sources with faint *K*-band counterparts (e.g., Chambers et al. 1996; Blundell et al. 1998). Follow-up optical spectroscopy detected faint Lyα emission from the host galaxy at a redshift of 5.1989 ± 0.0006 (van Breugel et al. 1999; Venemans et al. 2004). On the basis of its compact (1.″3) radio morphology, underluminous Lyα emission compared with other HzRGs, and rest-frame 350 nm emission composed of several clumpy optical features, it was suggested that TN J0924−2201 is a young, primeval galaxy actively forming the bulk of its stars (van Breugel et al. 1999). We initially chose TN J0924−2201 as a candidate for CO observations because, as the most distant known member of a sample of HzRGs, it is presumably one of the youngest (Blundell & Rawlings 1999). The existence of molecular gas would provide independent evidence for ongoing massive star formation, expected if we are probing its formation epoch. The southern declination ($\delta = -22°$) of this source makes observations from millimeter telescopes in the northern hemisphere difficult, and its redshift moves all CO transitions out of any Very Large Array (VLA) band. We used the new wide-bandwidth 1.2 cm and 3 mm receivers on the Australia Telescope Compact Array (ATCA) to search for CO (1–0) and CO (5–4) with $\nu_{\rm rest} = 115.2712$ and 576.2677 GHz, respectively.

3. ATCA OBSERVATIONS

Observations were carried out with the ATCA during 2004 August and September. The ATCA is an array of six 22 m antennas with baselines ranging from 30 m to 6 km and capable of east-west, north-south, and hybrid array configurations. We utilized the maximum available bandwidth of the current correlator with 128 MHz/64 channel configurations for two adjacent intermediate-frequency (IF) bands. The spectral resolution of this configuration is 4.4 MHz. For the CO (1–0) observations, we used the hybrid H168 array,[5] tuning the IFs to 18.561 and 18.631 GHz, respectively, allowing an overlap

[5] The size of the naturally weighted restoring beam in the H168 array at 18.6 GHz is 14.″5 × 10.″1, or 90 × 63 kpc.

TABLE 1

OBSERVED PHYSICAL PARAMETERS OF TN J0924−2201

Parameter	18.6 GHz Continuum	CO (1–0) Line	CO (5–4) Line
Peak (mJy beam^{-1})	0.71 ± 0.03	0.52 ± 0.12	7.8 ± 2.7
Width (km s^{-1})	...	250–400	200–300
I_{CO} (Jy km s^{-1})	...	0.087 ± 0.017[a]	1.19 ± 0.27
ΔR.A.$_{J2000.0}$ (arcsec)[b]	−0.7 ± 0.7	1.5 ± 2.1	−1.0 ± 1.3
Δdecl.$_{J2000.0}$ (arcsec)[b]	0.3 ± 0.7	4.5 ± 1.7	−2.8 ± 1.2

[a] The weaker feature in the CO (1–0) spectrum has not been included in this measurement because within the 300–400 km s^{-1} velocity range, there are several other similar features in the image that decrease its significance. If this feature were included, the velocity-integrated flux density of the CO (1–0) emission would be 0.12 ± 0.03 Jy km s^{-1}.

[b] These positions are offsets from high-resolution VLA observations: R.A.$_{J2000.0}$ = 09^{h}24^{m}19^s.92, decl.$_{J2000.0}$ = −22°01′41″.5 (van Breugel et al. 1999). Positive offsets are north and east of the radio galaxy position.

region (after bandpass correction) of 20 MHz. This setup benefitted from a simultaneous velocity coverage of 2500 km s^{-1} and resolution of 72 km s^{-1}. System temperatures ranged from 30 to 50 K, and phase stability was within ±20° over the course of the observations. Phase, amplitude, bandpass, and astrometric calibration were acquired by short observations of PKS B0919−260 every 12–25 minutes depending on the weather. Absolute flux density calibration was ensured by snapshot observations of Mars. We estimate the calibration to be accurate to better than ±20%.

The observational setup was repeated in the H75 array[6] with the IFs tuned to 92.853 and 92.921 GHz, respectively, for the CO (5–4) transition. System temperatures (measured once per hour using a 300 K mechanical paddle moved over the feed horn) ranged from 200 to 350 K, and phase stability was mostly within ±50° over the course of the observations. Phase and amplitude calibration were based on observations of PKS B0834−201 every 12 minutes, and the bandpass was determined by 10 minute observations of either PKS B1253−055 or PKS B0537−441. The rms error in the pointing ranged from 3″ to 7″ depending on the antenna (the primary beam at 93 GHz is 31″). We periodically observed the 0.5 Jy quasar PKS B0925−203, less than 2° from TN J0924−2201, to verify the calibration and astrometry. We estimate the flux scale to be accurate to better than ±30%. Data reduction was carried out in accordance with standard ATCA calibration procedures for millimeter observing.[7] Overall, 40 and 35 hr of observing time were employed at 18.6 and 92.9 GHz, respectively, to carry out this detection experiment. Table 1 gives a summary of our results.

4. RESULTS

4.1. CO (1–0)

The CO (1–0) line is detected in at least five independent channels covering ~400 km s^{-1} and shown in Figure 1. We subtracted a 0.71 mJy continuum in the *u*-*v* plane using a first-order spectral baseline fit. The continuum image is shown in gray scale in Figure 2. The velocity-integrated, continuum-subtracted, flux density is 0.087 ± 0.017 Jy beam^{-1} km s^{-1}, and the corresponding intrinsic CO line luminosity is L'_{CO} = (1.2 ± 0.26) × 10^{11} K km s^{-1} pc^2. There are two kinematic features apparent in the spectrum: the brighter, dominant, emission centered at v = 150 km s^{-1} (z = 5.202 ± 0.001) and a weaker feature lying ~200 km s^{-1} redward. Deeper observations

[6] The size of the naturally weighted restoring beam in the H75 array at 92.8 GHz is 5″.9 × 4″.7, or 37 × 30 kpc.

[7] See http://www.atnf.csiro.au/computing/software/miriad.

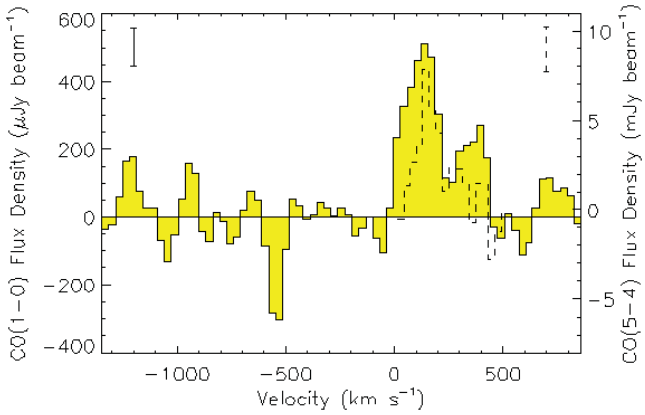


FIG. 1.—Spectra of the continuum-subtracted CO (1–0) (*shaded region*) and CO (5–4) (*dashed line*) transitions, through the peak of their respective velocity-integrated emission shown in Fig. 2. The CO (1–0) spectrum is unbinned (32 km s^{-1} bins; spectral resolution 72 km s^{-1}), while the CO (5–4) spectral channels have been rebinned into 30 km s^{-1} bins (original spectral resolution 15 km s^{-1}). The velocity axis is defined with respect to the Lyα-derived redshift of z = 5.1989, and the bars in the top left and right corners show the rms noise level in the CO (1–0) and CO (5–4) cubes, respectively.

are required to determine if the weaker feature is real. As commonly observed, the CO lies redward of the Lyα-derived redshift (see Table 1 in Klamer et al. 2004). There is no conclusive evidence for spatially extended gas, but the velocity-integrated emission (Fig. 2) appears to be offset to the north of the radio galaxy by 4″.5 ± 1″.7 (28 ± 11 kpc). At this stage, we do not consider this offset to be significant, since it is much less than a beam size away from the radio galaxy position. For comparison, the position angle of the projected radio axis is 29° (see Fig. 2). Deeper observations with higher spatial resolution are required to better constrain the spatial extent of this gas.

4.2. CO (5–4)

At 93 GHz, our instantaneous velocity coverage was only 600 km s^{-1}, with a spectral resolution of 15 km s^{-1}. The re-

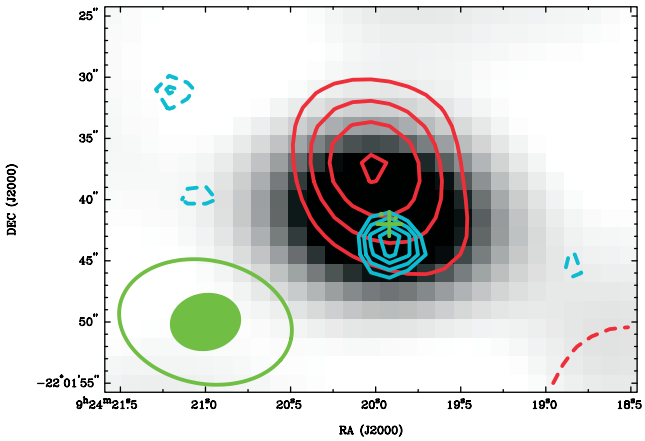


FIG. 2.—Gray-scale 18.6 GHz continuum image with CO (1–0) and CO (5–4) velocity-integrated emission overlaid in red and cyan, respectively. The continuum flux density is 0.71 ± 0.03 mJy, the CO (1–0) contour levels are ±2, 3, 4, 5 × σ, where σ = 0.017 Jy beam^{-1} km s^{-1}, and the CO (5–4) contour levels are ±2.5, 3, 3.5, 4 × σ, where σ = 0.27 Jy beam^{-1} km s^{-1}. The sizes of the 18 GHz (*open ellipse*) and 93 GHz (*filled ellipse*) restoring beams are shown in the bottom left corner; the plus sign shows the optical position of the radio galaxy. The radio lobes, illustrated with filled circles, extend 1″.3 along a position angle of 29°.

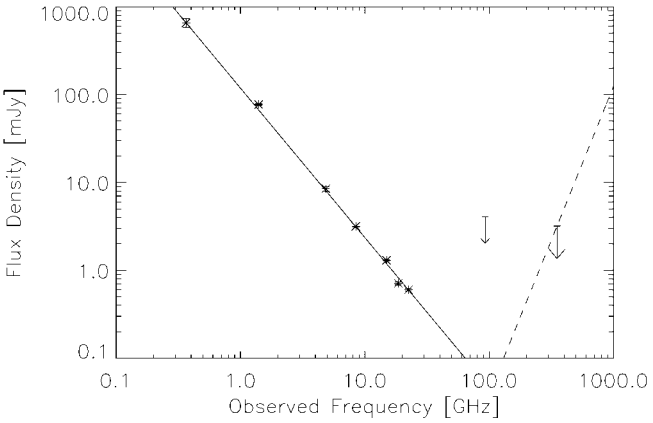


FIG. 3.—Radio-to-submillimeter spectral energy distribution of TN J0924−2201. The stars are radio observations from the Texas, NVSS, and PMN radio sky surveys along with pointed VLA observations and the ATCA 18.6 GHz continuum point from this work. The solid line is a power law with spectral index $\alpha = -1.7$. The 352 GHz upper limit is from Reuland et al. (2004), and the dashed line shows the Rayleigh-Jeans portion of a modified blackbody spectrum, normalized to the 352 GHz (850 μm) limit, with $T = 50$ K and $\beta = 1.5$. The upper limit at 93 GHz is from this Letter using the CO (5–4) flux density averaged over the range 0–300 km s^{-1}.

sultant spectrum is shown in Figure 1, and the emission profile integrated from 0 to 300 km s^{-1} is shown in Figure 2. Although the zero level in the profile is well determined from offset positions in the image, our bandwidth is only marginally wider than the line width, so we have to consider the possibility of a spectral baseline offset due to continuum emission from the radio galaxy. However, the flux density we observe is more than 100 times that expected from the continuum. This is illustrated by the radio-to-submillimeter spectral energy distribution shown in Figure 3. Extrapolating the nonthermal synchrotron spectrum with a spectral index of $\alpha = -1.7$, we expect a contribution of <0.04 mJy, while extrapolating from the 352 GHz Submillimeter Common-User Bolometric Array (SCUBA) limit assuming a modified blackbody spectrum with $\beta = 1.5$ and $T = 50$ K, we expect the contribution due to thermal dust radiation to be <0.01 mJy. The most likely source of the 93 GHz emission is therefore the redshifted CO (5–4) transition at $z = 5.202$. The velocity-integrated flux density is 1.19 ± 0.27 Jy beam^{-1} km s^{-1}, corresponding to $L'_{\rm CO} = (4.3 \pm 1.0) \times 10^{10}$ K km s^{-1} pc^2. Again, the emission appears offset from the radio galaxy position, the peak lying $2\farcs8 \pm 1\farcs2$ (18 ± 8 kpc) south. Again, the positional offset is less than a beam size. Deeper observations are required to constrain the spatial extent of the molecular gas, including whether there are physically distinct gas-emitting regions.

5. PHYSICAL PROPERTIES OF THE MOLECULAR GAS

5.1. *Mass Estimates*

CO observations are translated into total H_2 mass estimates, assuming that the observed CO traces molecular clouds on large scales and that the molecular gas mass dominates the total dynamical mass of the galaxy. These mass estimates are uncertain at best, but to facilitate comparison with observations from other HzRGs, we assume $M(H_2)/L'_{\rm CO} \equiv \alpha = 0.8\,M_\odot$ (K km s^{-1} pc^2)$^{-1}$ as measured for nearby ultraluminous infrared galaxies (Downes & Solomon 1998). Since molecular clouds provide both the fuel and the site for the next generation of star formation, our result implies that there is $\sim 10^{11}\,M_\odot$ of available gas from which to manufacture the next stellar generation. This estimate is consistent with $M(H_2)$ estimates of other HzRGs like 4C 60.07 (Greve et al. 2004; Papadopoulos et al. 2000) and B3 J2330+3927 (De Breuck et al. 2003). There is no direct evidence to indicate that TN J0924−2201 is gravitationally lensed. However, if lensing is important, then $L'_{\rm CO}$, and hence $M(H_2)$, are upper limits only.

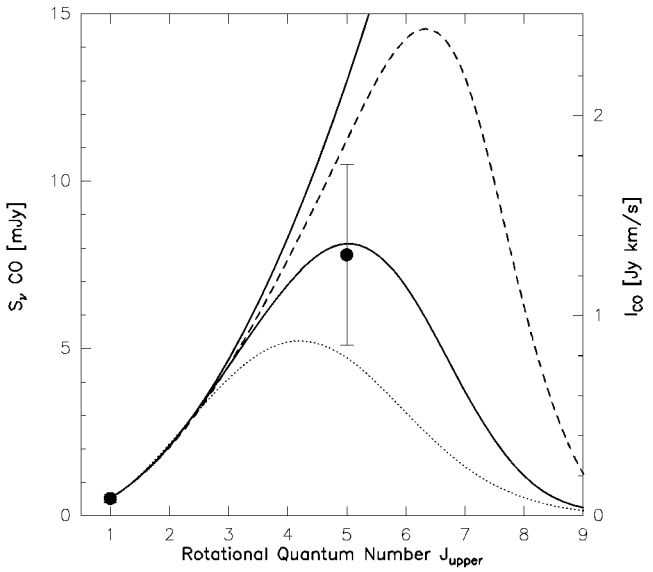


FIG. 4.—CO ladder with LVG models overlaid. The best match to the observations is $\log[n(H_2)] = 3.3$, $T_{\rm kin} = 50$ K, and $r > 2.0$ kpc (*solid line*). Also in agreement with the observations are $\log[n(H_2)] = 4.0$, $T_{\rm kin} = 30$ K, and $r > 2.9$ kpc (*dashed line*) and $\log[n(H_2)] = 2.7$, $T_{\rm kin} = 150$ K, and $r > 2.2$ kpc (*dotted line*). The condition for optically thick, thermally excited gas is the solid, parabolic fit. The error bars are 1 σ noise estimates and do not include the uncertainty in the absolute flux scale (§ 3).

5.2. *Temperature and Density from Large Velocity Gradient Modeling*

The ratio of the peak flux densities would be equal to the square of the ratio of the upper transition levels (1/25) in the event that both lines are optically thick and thermally excited. Under the assumption of optically thick gas, the ratio we measure is $1/(15 \pm 9)$, which suggests the CO (5–4) transition is subthermal; however, the errors are large. We have used a standard single-component large velocity gradient (LVG) code, with a typical CO-to-H_2 abundance $X[{\rm CO}]/(dv/dr) = 8 \times 10^{-5}$ (km s^{-1})$^{-1}$ pc, to further constrain the physical properties of the molecular gas. A good match to the observations is given by $\log[n(H_2)] = 3.3$ [where $n(H_2)$ is measured in units of cm^{-3}], $T_{\rm kin} = 50$ K, and $r > 2.0$ kpc, but other density/temperature combinations are also consistent with the observed fluxes (see Fig. 4). Observations of CO transitions higher than CO (5–4) are required to constrain the excitation conditions of the gas. If the observed offsets between the CO (1–0) and CO (5–4) transitions reflect physically distinct CO emitting regions, then the excitation conditions presented here become invalid.

5.3. *Where Is the Dust?*

At present, the most efficient technique for detecting high-redshift molecular gas is to preselect the dustiest objects, as determined from their large rest frame far-infrared luminosities using (sub)millimeter sensitive instruments like SCUBA on the James Clerk Maxwell Telescope or MAMBO on the IRAM 30 m telescope. This also means that current samples are biased

toward objects with the largest dust-to-gas ratios ($L_{\rm FIR}/L'_{\rm CO} \sim 300\ L_\odot\ {\rm K}^{-1}\ {\rm km}^{-1}\ {\rm s}\ {\rm pc}^{-2}$; Carilli et al. 2004). For comparison, the median ratio is 160 for nearby ultraluminous infrared galaxies with $L_{\rm FIR} \gtrsim 10^{12}\ L_\odot$ (Solomon et al. 1997) and about 50 for nearby luminous infrared galaxies with $10^{11}\ L_\odot < L_{\rm FIR} \lesssim 10^{12}\ L_\odot$ (Gao & Solomon 2004). The selection bias at high redshift is further compounded by the fact that initial CO detections are usually made in $J \geq 3$ order lines, which prejudices the sample against regions of low-density molecular gas where the higher order transitions are subthermally excited.

Five of the six published CO detections of HzRGs constitute the most far-infrared–luminous $z > 1$ radio galaxies recently surveyed with SCUBA (Reuland et al. 2004). In this sample, approximately 50% of the 24 observed galaxies were not detected; TN J0924−2201 featured among these nondetections with $L_{850\ \mu{\rm m}} < 1 \times 10^{24}$ W Hz^{-1}, 5 times underluminous compared to the CO-detected HzRGs in the sample. Therefore, TN J0924−2201 will have a dust-to-gas ratio at least 5 times smaller than the current sample of high-redshift galaxies, similar to the nearby luminous infrared galaxy population. The only other CO emitter at high redshift not selected on the basis of far-infrared emission—that we are aware of—is 53W002 at $z = 2.394$ (Yamada et al. 1995; Scoville et al. 1997; Alloin et al. 2000). This source has a 3 σ upper limit of 4.3 mJy at 850 μm (Archibald et al. 2001), corresponding to $L_{850\ \mu{\rm m}} < 7 \times 10^{24}$ W Hz^{-1}. An a posteriori detection of the dust content in 53W002 (1.7 ± 0.4 mJy at 1.3 mm; Alloin et al. 2000) suggests that a similar observation of TN J0924−2201 may also reveal its dust content. Thus, 53W002 and TN J0924−2201 may be representative of a population of high-redshift sources that remain undetected owing to current selection techniques.

6. COEVOLUTION OF A CENTRAL DOMINANT AND A PROTOCLUSTER

At $z = 5.2$, the universe is only about a billion years old—time enough, however, to build a supermassive black hole, trigger powerful radio jets, and produce a stellar population capable of enriching the interstellar medium with $\sim 10^7\ M_\odot$ of CO (assuming an abundance of CO relative to H_2 of $Z_{\rm CO} = 10^{-4}$). This rapid enrichment could be facilitated in part by the powerful radio jets themselves propagating into overdensities in the primordial gas and shock-inducing massive star formation (Klamer et al. 2004; Bicknell et al. 2000). Venemans et al. (2004) recently postulated that TN J0924−2201 resides within a protocluster environment after discovering six Lyα emitters in a $6\farcm8 \times 6\farcm8$ field (2.6 × 2.6 Mpc) around the radio galaxy—the typical scale size for nearby rich clusters (Abell 1958). Our CO observations substantiate a 5 yr old hypothesis that TN J0924−2201 is a young forming galaxy, potentially the primeval central dominant galaxy of a rich cluster. Thus, it seems that cD galaxies may form with their host environments from the earliest times in the universe.

Big thanks go to everyone who made the 12 and 3 mm ATCA upgrades possible. Thanks also to Chris Carilli for the VLA observations, which we have incorporated into Figures 2 and 3, and Christian Henkel, who originally wrote the LVG code. I. J. K. acknowledges receipt of an Australian Postgraduate Award and CSIRO Postgraduate Scholarship. The ATCA is part of the Australia Telescope, which is funded by the Commonwealth of Australia for operation as a National Facility managed by CSIRO.

REFERENCES

Abell, G. O. 1958, ApJS, 3, 211
Alloin, D., Barvainis, R., & Guilloteau, S. 2000, ApJ, 528, L81
Archibald, E. N., Dunlop, J. S., Hughes, D. H., Rawlings, S., Eales, S. A., & Ivison, R. J. 2001, MNRAS, 323, 417
Bicknell, G. V., Sutherland, R. S., van Breugel, W. J. M., Dopita, M. A., Dey, A., & Miley, G. K. 2000, ApJ, 540, 678
Blundell, K. M., & Rawlings, S. 1999, Nature, 399, 330
Blundell, K. M., Rawlings, S., Eales, S. A., Taylor, G. B., & Bradley, A. D. 1998, MNRAS, 295, 265
Carilli, C. L., Bertoldi, F., Walter, F., Menten, K. M., Beelen, A., Cox, P., & Omont, A. 2004, preprint (astro-ph/0402573)
Carilli, C. L., Röttgering, H. J. A., van Ojik, R., Miley, G. K., & van Breugel, W. J. M. 1997, ApJS, 109, 1
Chambers, K. C., Miley, G. K., van Breugel, W. J. M., Bremer, M. A. R., Huang, J.-S., & Trentham, N. A. 1996, ApJS, 106, 247
De Breuck, C., van Breugel, W., Röttgering, H. J. A., & Miley, G. 2000, A&AS, 143, 303
De Breuck, C., et al. 2003, A&A, 401, 911
Downes, D., & Solomon, P. M. 1998, ApJ, 507, 615
Fan, X., et al. 2003, AJ, 125, 1649
Gao, Y., & Solomon, P. M. 2004, ApJ, 606, 271
Greve, T. R., Ivison, R. J., & Papadopoulos, P. P. 2004, A&A, 419, 99
Klamer, I. J., Ekers, R. D., Sadler, E. M., & Hunstead, R. W. 2004, ApJ, 612, L97
Le Fèvre, O., Deltorn, J. M., Crampton, D., & Dickinson, M. 1996, ApJ, 471, L11
Lilly, S. J., & Longair, M. S. 1984, MNRAS, 211, 833
McCarthy, P. J., Spinrad, H., Dickinson, M., van Breugel, W., Liebert, J., Djorgovski, S., & Eisenhardt, P. 1990, ApJ, 365, 487
Papadopoulos, P. P., Röttgering, H. J. A., van der Werf, P. P., Guilloteau, S., Omont, A., van Breugel, W. J. M., & Tilanus, R. P. J. 2000, ApJ, 528, 626
Pascarelle, S. M., Windhorst, R. A., & Keel, W. C. 1998, AJ, 116, 2659
Pentericci, L., Röttgering, H. J. A., Miley, G. K., McCarthy, P., Spinrad, H., van Breugel, W. J. M., & Macchetto, F. 1999, A&A, 341, 329
Pentericci, L., et al. 2000, A&A, 361, L25
Reuland, M., Röttgering, H., van Breugel, W., & De Breuck, C. 2004, MNRAS, 353, 377
Scoville, N. Z., Yun, M. S., Windhorst, R. A., Keel, W. C., & Armus, L. 1997, ApJ, 485, L21
Solomon, P. M., Downes, D., Radford, S. J. E., & Barrett, J. W. 1997, ApJ, 478, 144
Spergel, D. N., et al. 2003, ApJS, 148, 175
Stevens, J. A., et al. 2003, Nature, 425, 264
van Breugel, W. J. M., De Breuck, C., Stanford, S. A., Stern, D., Röttgering, H., & Miley, G. 1999, ApJ, 518, L61
van Breugel, W. J. M., Stanford, S. A., Spinrad, H., Stern, D., & Graham, J. R. 1998, ApJ, 502, 614
Venemans, B. P., et al. 2004, A&A, 424, L17
Villar-Martín, M., Vernet, J., di Serego Alighieri, S., Fosbury, R., Humphrey, A., & Pentericci, L. 2003, MNRAS, 346, 273
Walter, F., et al. 2003, Nature, 424, 406
Yamada, T., Ohta, K., Tomita, A., & Takata, T. 1995, AJ, 110, 1564